4-18-2011

A Comparison of Elastic Modulii of Femurs from Genetically Modified Mice: Three-Point Bending Experiments and a Correction Factor Approach

Meagan Maureen Buechel

To the University Council:

The Thesis Committee for Meagan Maureen Buechel certifies that this is the final approved version of the following thesis: “A Comparison of Elastic Modulii of Femurs from Genetically Modified Mice: Three-Point Bending Experiments and a Correction Factor Approach.”

_____
Esra Roan, Ph.D., Major Professor

We have read this thesis and
recommend its acceptance:

_____
Gladius Lewis, Ph.D.

_____
Hsiang H. Lin, Ph.D.

Accepted for the Graduate Council:

_____
Karen D. Weddle-West, Ph.D.
Vice Provost for Graduate Programs

A COMPARISON OF ELASTIC MODULII OF FEMURS FROM GENETICALLY MODIFIED MICE: THREE-POINT BENDING EXPERIMENTS AND A CORRECTION FACTOR APPROACH

by

Meagan Maureen Buechel

A Thesis

Submitted in Partial Fulfillment of the

Requirements for the Degree of

Master of Science

Major: Mechanical Engineering

The University of Memphis

May 2011

ACKNOWLEDGEMENTS

I would like to express my sincere gratitude to several people who have greatly contributed to the completion of this project. First of all, I would like to thank my friends and family for their unconditional support throughout my educational career. Thank you all for giving me the motivation to pursue this degree. I also want to thank Dr. Zhousheng Xiao for providing the murine femurs for this work. In addition, thank you to my committee members, Dr. Gladius Lewis and Dr. Hsiang Lin, for directing the course of my project. Finally, I want to thank my advisor, Dr. Esra Roan, who has helped me tremendously.

ABSTRACT

Buechel, Meagan M. M.S., The University of Memphis. May 2011
“A Comparison of Elastic Modulii of Femurs from Genetically Modified Mice: Three-Point Bending Experiments and a Correction Factor Approach,”
Major Professor: Esra Roan, Ph.D.

Studies into how genetic modifications affect bone development may help research into new treatments for bone diseases. In order to understand whether these treatments are effective, bones should be mechanically evaluated, because ultimately they support large mechanical loads. Three-point bend testing has been widely utilized in the mechanical evaluation of whole, long bones since these bones fail mostly in bending. The accuracy of the mechanical properties obtained from these tests using the Euler-Bernoulli beam equations is questionable; due to the complexity of the bending mechanics of long bones. Therefore, in this work, a correction factor approach was utilized to measure, correct, and compare the elastic modulus of femurs of mice with one of three genetic modifications to that of the control group. Experiments and parametric finite element models were utilized to show that statistically significant differences exist among the bones from one of the genetic groups compared to the others.

TABLE OF CONTENTS

LIST OF ABBREVIATIONS

LIST OF TABLES

LIST OF FIGURES

CHAPTER 1: INTRODUCTION

Studies into how genetic modifications affect bone development may help define a new target for developing growth agents to treat bone disorders. There are numerous bone disorders and diseases affecting people of varying ages, such as osteoporosis. Osteoporosis alone affects more than 40 million people in the United States (NIH, 2011).

Osteoporosis and other bone disorders are degenerative and alter the mechanical properties of the bone. Genetic studies are effective in studying these disorders. Two genes, Pkd1 and Kif3a, are of particular interest in this case due to previous results that have shown that loss of Pkd1 function results in abnormal bone development at the osteoblast level (Xiao & Quarles, 2010). No studies have been done to test the effects of loss of Kif3a function on bone development.

Imaging studies can provide substantial information regarding the bone, such as, densitometric and geometric properties. Ultimately; however, bones need to be mechanically evaluated, because they support large mechanical loads. To assess the mechanical properties of the long bones and to enable accurate comparisons across studies, there is a need for the standardization of mechanical testing procedures. Currently, no such standardization exists. In previous studies, a variety of techniques, such as compressive, tensile, torsional, four-point bending and three-point bending tests have been used (Bell, 1941). These provide various mechanical parameters for comparison, but elastic modulus, E, is a fundamental one that can be obtained from most mechanical

tests and it is indicative of a material's resistance to deformation. Of the mechanical testing methods, three-point bending is a simple, reproducible test, making it the preferred method of mechanical testing of the long bones of small animals, which also can provide an elastic modulus (Burstein & Frankel, 1972).

The accuracy of the E obtained from bending tests in general is questionable due to several factors, which all relate to the fact that the underlying assumptions of the fundamental Euler-Bernoulli bending mechanics equations are violated. First, the test assumes that the geometry and thickness of the bones is uniform throughout its length. Second, with an aspect ratio (length/outer diameter) less than 20, the bone is subjected to not just bending, but also to shearing. Third, local deformations, which are evident near the supports, are neglected. Due to these factors that violate assumptions, the results derived from the three-point bend tests with the use of the simple Euler-Bernoulli beam framework give a much lower calculated elastic modulus than obtained using other techniques (Kourtis & Beaupre, 2011; Turner, 1993). Previous workers have developed bending mechanics corrections, but these are complex and, so, are challenging to use (Hutchinson, 2001; Schriefer, 2005).

In the present work, a numerical approach was adopted that allows the use of the simpler mechanics framework for three-point bending through the derivation of a correction factor dependent on the geometry and material properties of the long bone itself. Three-point bending experiments, finite element analysis (FEA), and optimization algorithms were utilized to determine the mechanical response and geometry of the genetically modified murine femurs, to

correct this measured response, and to compare inherent differences due to genetic modifications.

CHAPTER 2: BACKGROUND

In this chapter, the basic concepts of bone disorders, murine anatomy, and mechanical testing techniques are presented. The elastic modulus of various murine bones at different ages found with the various techniques will also be presented. The background also provides a brief introduction to the finite element (FE) method.

Bone Disorders

Osteoporosis is a common type of bone disease, especially in women over 50 years of age. Osteoporosis is the thinning of bone tissue and loss of bone density over time. It occurs when the body fails to form enough new bone, a greater amount of the old bone is reabsorbed by the body than the newly formed bone, or both. As a person ages, calcium and phosphate may be reabsorbed into the body from the bones, which makes the bone tissue weaker. This can result in brittle, fragile bones that are more prone to fractures, even without injury. Usually, the loss occurs gradually over years. Many times, a person will have a fracture before becoming aware that the disease is present. By the time a fracture occurs, the disease is in its advanced stages and damage is severe (NCIB, 2010). Osteopenia refers to bone mineral density that is lower than normal but not low enough to be classified as osteoporosis. Having osteopenia greatly increases a person's risk of developing osteoporosis in later years (Osteopenia Health Center, 2008).

Osteogenesis imperfecta (OI) is a condition characterized by extremely fragile bones. OI is a congenital disease. It is frequently caused by a defect in the

gene that produces type 1 collagen protein, an important building block of bone. There are many different defects that can affect this gene. The severity of OI depends on the specific gene defect. Most cases of OI are inherited, although some cases are the results of new genetic mutations (NCIB, 2009).

For these types of disorders, two of the genes currently being studied are Pkd1 and Kif3a. Autosomal (pertaining to a chromosome) dominant polycystic kidney disease is caused by inactivating mutations of Pkd1 (polycystic kidney disease 1) gene. It has previously been shown that loss of Pkd1 (polycystin-1) function in mice results in abnormal bone development and osteopenia due to the impaired differentiation of osteoblasts (cells that are responsible for bone formation). Kif3a (kinesin family member 3a) gene codes the transport protein Kif3a, which maintains primary cilia. Mutations of Kif3a cause autosomal recessive polycystic kidney disease. Kif3a is used in this study to determine if the effect of bone-specific deletion of Kif3a can be compared to that of osteoblast-specific deletion of Pkd1. Overall, polycystins in bone may define a new target for developing anabolic agents to treat osteoporotic disorders (Xiao et al., 2006; Xiao et al., 2010; Xiao, Magenheimer, & Quarles, 2008; Xiao & Quarles, 2010).

Murine Anatomy

Mice are common experimental animals primarily because they are mammals, and also because they share a high degree of homology (a fundamental similarity based on common descent) with humans. The murine genome has been sequenced and virtually all mouse genes have human homologs. Other reasons mice are used in laboratory research are that they are

small, inexpensive, easily maintained, and can reproduce quickly (The University of Iowa, 2006). Figure 1 gives the basic murine skeletal anatomy, highlighting three of the commonly tested long bones.

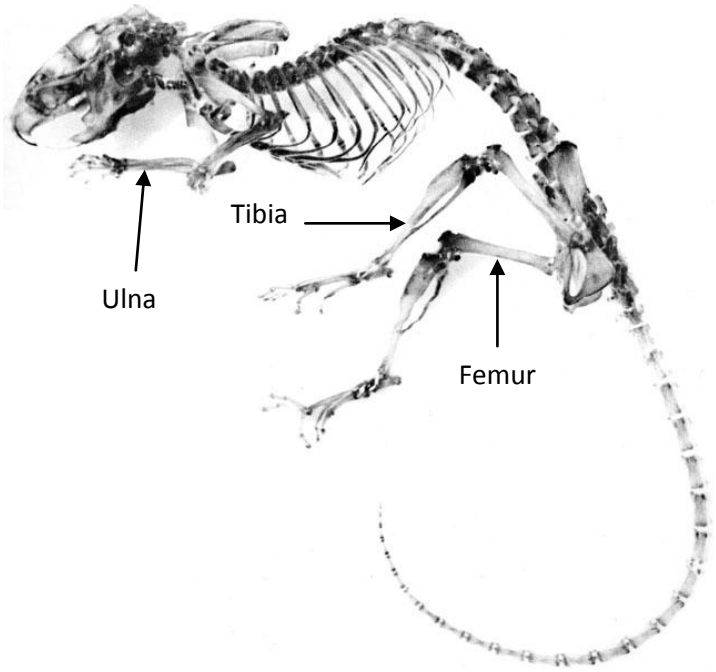

Figure 1. Basic murine skeletal anatomy (Cook, 2008).

There are five protuberances in the murine femur: the head, the greater trochanter, the lesser trochanter, the third trochanter, and the lower extremity. The lower extremity, or distal end, of the femur is made up of the medial and lateral fabella and the medial and lateral condyle (Figure 2) (Femur, 2011).

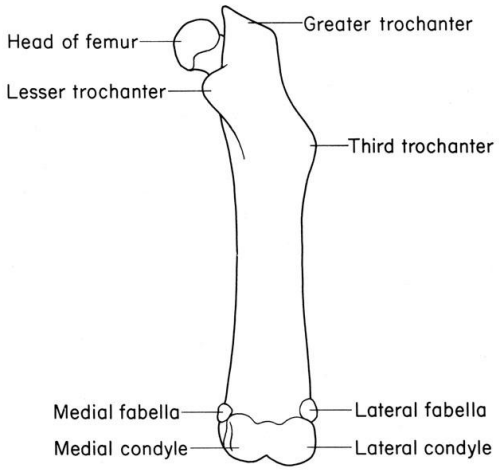

Figure 2. Anatomy of a murine femur (Cook, 2008).

Mechanical Testing of Bones

Three-Point Bending. Three-point bending tests are commonly used to assess the material and structural properties of long bones. One purpose of such a test is to determine the elastic modulus, E, which is typically obtained by use of an algebraic equation derived from elementary beam theory. The main advantage of a three-point bending test is the ease of testing. However, this method also has many disadvantages, as mentioned in the previous section including the fact that the test results are sensitive to the specimen dimensions, loading geometry, and strain rate (Simkin & Robin, 1973). These all relate to the violation of underlying assumptions of the elementary beam theory. More complex theories have been developed that address the introduction of shear; however, the concerns over geometry and local deformations still remain unresolved in these more complex frameworks (Hutchinson, 2001; Schriefer et al., 2005).

Three-point bending occurs when three forces acting on a beam produce two equal moments, as shown in Figure 3. Each bending moment, M, is the product of one of the two reaction (support) forces and its perpendicular distance from the axis of rotation, the point of application of the middle force, F. The deflection, δ, of the beam is directly proportional to the (beam length, L)^3. The shear, V, is constant in absolute value, that is, half the central load. If loading continues to the yield point, the structure should break at the application point of the middle force, assuming that the structure is homogeneous and symmetrical (Three Point Flexural Test, 2011).

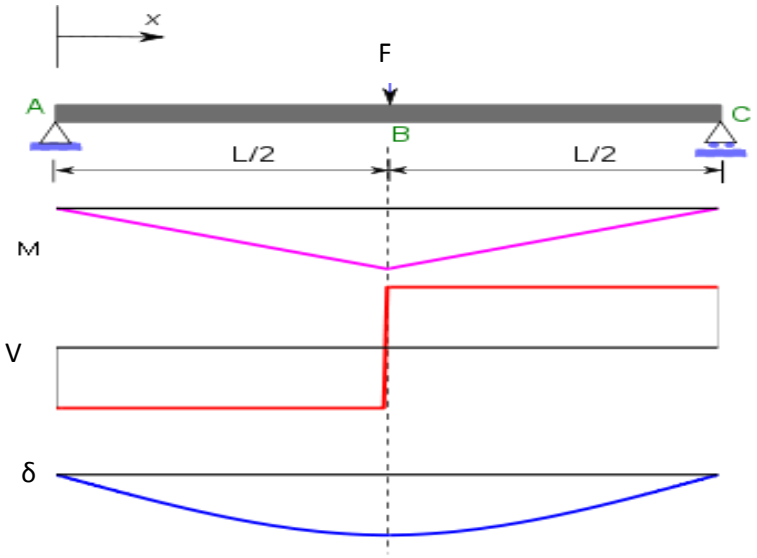

Figure 3. The bending moment (M), shear force (V), and deflection (δ) diagrams for a beam subject to a central point load (F) during three-point bending (Bending, 2011).

Other Testing Techniques. There are other mechanical testing techniques that can be used to determine elastic modulus, such as four-point bending test, nanoindentation, electronic speckle pattern interferometry (ESPI), tension test, compression test, and torsion test. Four-point loading is advantageous because it produces pure bending between two loading points, which ensures that transverse shear stresses are zero (Martens, van Audekercke, de Meester, & Mulier, 1986). However, it requires that the force at each loading point be equal; this requirement is simple to achieve in regularly shaped specimens but difficult to achieve in whole bone samples (Draper & Goodship, 2003; Saffar, JamilPour, & Rajaai, 2009).

The nanoindentation technique was developed in the 1970s to measure the hardness of small volumes of materials. This technique is limited due to large and varied tip shapes, with indenter rigs that do not have very good spatial resolution, which makes comparison across experiments difficult. This technique provides nano-scale response of the bone which may not be a realistic measure when the aim is to obtain gross mechanical response of the long bone (Nanoindentation, n.d.; Tang, Hgan, & Lu, 2007).

ESPI is a technique, in which laser light, together with video detection, recording and processing, s used to visualize static and dynamic displacements of components. When working with murine femurs, micro-computer tomography (μCT) is often used as the video detection tool (Chattah, Sharir, Weiner, & Shahar, 2009). Other common methods used for mechanical testing of whole

and sectioned bones are tension, compression, and torsion tests, which are standard mechanical testing techniques.

Literature Results. A sample of values of the elastic modulus of murine bones, obtained using various techniques, is presented in Table 1.

Table 1
Sample of Elastic Modulus Results for Murine Bone Obtained Using Various Mechanical Testing Techniques

Technique	Bone	Age (weeks)	Elastic Modulus (GPa)	Source
Three-point bending	Femur	10	3.42 ± 0.21 - 10.87 ± 0.29	Wergedal et al., 2005
Three-point bending	Femur	-[a]	1.92 ± 0.52	Jamsa et al., 1998
Three-point bending	Tibia	-[a]	3.75 ± 1.13	Jamsa et al., 1998
Compression	Ulna	20	13.3 ± 0.7 - 15.9 ± 0.4	Robling et al., 2002
ESPI	Femur	4	8.6 ± 1.4 - 10.4 ± 0.9	Chattah et al., 2009
Nanoindentation (dry)	Femur	-[a]	14.22 ± 2.61	Tang et al., 2007
Tension	Femur	14	15.9 ± 8.1	Miller et al., 2007

[a] Age not given in report.

Finite Element Analysis in Biomechanics

The finite element analysis (FEA) method has been widely used in biomechanical analysis of stresses and strains of bone since its introduction to orthopedics in 1972 (Brkelmans, Poort, & Slooff, 1972). FEA is a powerful computational method capable of evaluating stresses of an entire structure even if the structure has a complex shape, loading and/or material behavior, as is experienced in the case of three-point bending of murine femurs. The stress

distribution is evaluated by using a computational model in which structural features, loading, geometry, material properties, boundary and material interface conditions, are described as mathematical equations. These mathematical equations are usually based on experimental data and simulate the actual structure to a degree. During the solution process, the structural descriptions are combined with equations based on the theories of solid mechanics to produce approximate numerical solutions (Huiskes & Chao, 1983).

To create a finite element (FE) model, first the geometry of the structure of interest has to be defined. In this continuum body, the unknown quantity (e.g., stress, pressure, temperature, etc.), also known as the field variable, is a function of infinitely many points in the continuum; thus, it is associated with infinitely many values or "unknowns." In order to arrive to an approximation of the problem, this geometrical model is then mathematically discretized, or divided, into small sub-regions, termed "elements," interconnected at specific points or nodes. By dividing the problem into an assembly of discrete elements, the continuum problem is reduced to a finite number of unknowns. The field variables can now be described in terms of approximating functions, also known as interpolation functions, which are assumed for the nodes of each element. Every element is then assigned properties (e.g., elastic modulus and Poisson's ratio) that describe its material behavior. Subsequently, boundary conditions are specified, these being known nodal values of the dependent variables. By simultaneously solving a system of equations, FEA ultimately yields a "piecewise" approximation of the mathematical equations for each element, and

then assembles these solutions to represent the problem as a whole (Huebner, Dewhirst, & Smith, 2001).

Accuracy and Validation of FE Models. The accuracy of an FE model depends on the capability of the collective elements, known as a mesh, to approximate the exact solution of the model. Theoretically, as the mesh density of any model approaches infinity, the solution obtained by using FEA converges to the exact solution. The accuracy of the model can be assessed by mesh convergence studies, in which the solution for the current mesh density is compared to solutions produced by increasingly refined meshes until convergence is reached (Huiskes & Chao, 1983).

Validation of the FE model may be defined as how accurately the mathematical equations for structural definitions assumed in the model simulate the real-life structure. Validation of FE models is usually achieved through comparison of experimental data to results of the FE analysis (Huiskes & Chao, 1983).

Element Types. An extensive library of elements is available in commercially-available FE software packages varying in shape, number of nodes, degrees-of-freedom, dimensionality, etc. Continuum solid elements are standard volume elements that can be used in a variety of linear stress analyses. Reduced integration elements converge non-monotonically, whereas elements which do not have reduced integration converge monotonically. Reduced integration reduces the amount of computational cost for analysis of a model, and it typically provides results which are more accurate (Abaqus, 2007).

In many types of structural analysis, contact can occur when the structure of interest either makes contact with itself or another structure. Contact problems in FEA can be generally classified into either a “rigid-to-flexible” contact or a “flexible-to-flexible” contact. Modeling of three-point bending is an example of a “rigid-to-flexible” contact problem, where the supports and the loading fixture are treated as rigid because they have a much higher stiffness relative to the murine femur they contact. In order to model contact in FEA, the possible interactions of bodies must be analyzed before the model is built. It is common to use surface-to-surface interactions (Mac Donald, 2007).

Parametric Studies and Error Functions. The correction factor approach is based on the hypothesis that the error in the elastic modulus extracted from the experiments depends with the use of Euler-Bernoulli beam equations on the true elastic modulus as well as on the geometric properties of the test member.

FE parametric studies have previously been used to determine error functions and to correct material property calculations for compression tests on soft tissue (Roan, 2007). The parameters of the compression experiments and the hyper-viscoelastic properties of the tissue complicated the extraction of the material properties from the experiments. This rendered the governing material property equations unusable until the correction from the error function was applied.

In summary, this work originates from multiple competing factors: the need and practicality of thee-point bending experiments and the major challenges

related to the complexity of these experiments in long bones from small animals. The useful nature of FE in addressing problems with nonlinearity is utilized in this work to compare the true mechanical properties of bones from genetically modified animals.

CHAPTER 3: MATERIALS AND METHODS

The aim of this work is to mechanically characterize murine femurs that are from genetically modified animals and to determine whether differences in the properties between the four experimental groups exist. Four experimental groups used in this study are: 1) Pkd1 heterozygous (JHet), 2) Kif3a heterozygous (KHet), 3) Pkd1 and Kif3a double heterozygous (KJHet), 4) wild-type control (WT). Because of concerns regarding the mechanics of three-point bending, a correction factor was determined using FEA for each bone. Due to the scope of this work, both computational and experimental activities were necessary.

Three-Point Bending of Murine Femurs

Forty-eight femurs from 6-week-old, male, mice were acquired for the three-point bend testing. Femurs were stored at 4°C prior to acquisition. After acquisition, the femurs were stored at 0°C, until being thawed in 1X phosphate buffered saline (PBS) 5 minutes prior to testing. The distance between the supports was held constant for all femurs at 6 mm (Figure 4) and the radius of supports was 0.5 mm. The femurs were tested using an Instron 33R (Instron, Norwood, MA) at a rate of 2 mm/sec to a 40% decline in maximum load (Jamsa, 1998; Schriefer, 2005). Load magnitude and displacement data were collected by the Bluehill® Materials Testing Software (Instron, Norwood, MA).

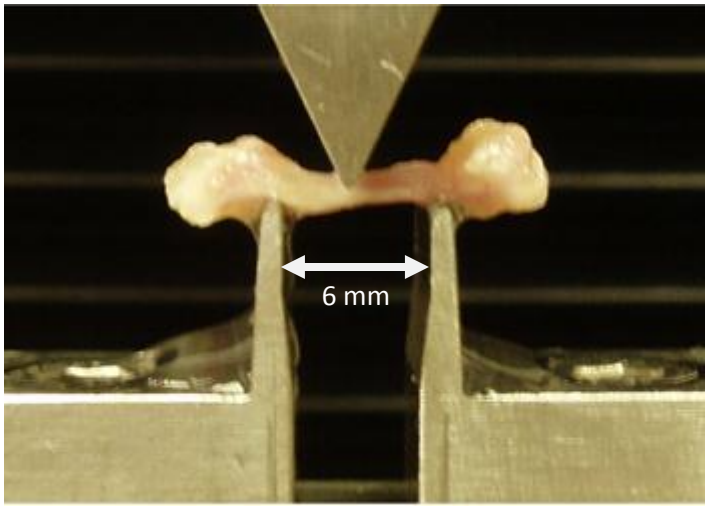

Figure 4. Photograph of a murine femur positioned for a three-point bending experiment test.

Collection of Geometric Parameters

For each femur, μCT data (1520 slices per femur) were imported into the imaging software, Amira (Pro Medicus Limited, Richmond, Australia), and saved in a DICOM file format. Measurements of the inner and outer diameters in both the x and y directions were taken using a DICOM viewer (Santa DICOM Viewer FREE, Santesoft, Athens, Greece). To increase the accuracy of the measurements, a threshold on the luminosity was applied with a lower limit of 1,000 and an upper limit of 1,500. For each specimen, three slices were measured and the averages were then used for the calculations. Figure 5 displays a sample scan that was used to obtain the diameters of the femurs. From this data, the moment area of inertia (*I*) was calculated using the expression (Cowin, 2001)

$$I = \frac{\pi}{64}(X_1 Y_1^3 - X_2 Y_2^3) \quad (3.1)$$

where X_1 and Y_1 are the outer diameters and X_2 and Y_2 are the inner diameters. After I was calculated it was combined with the force – displacement data from the three-point bending tests to calculate the apparent elastic modulus, E_{app}, using the following expression (Cowin, 2001)

$$E_{app} = \frac{FL^3}{48\delta I} \tag{3.2}$$

where F is the applied force, L is the span, and δ is the deflection.

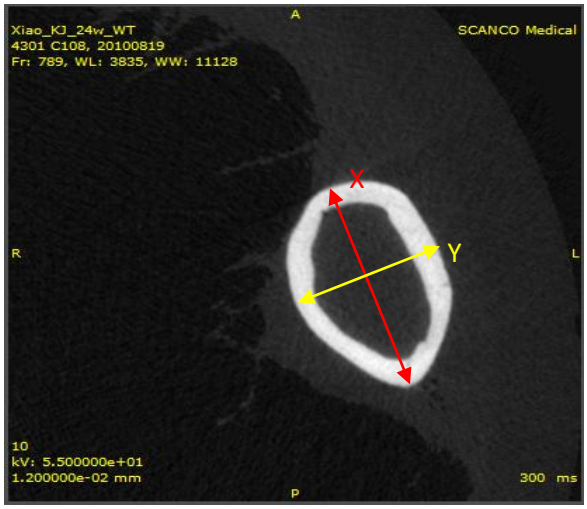

Figure 5. A sample micro-CT scan showing the orientation of the femur during mechanical testing.

Finite Element Modeling of the Femur

For each femur, μCT data (1520 slices per femur) were imported into the imaging software, Amira (Pro Medicus Limited, Richmond, Australia), for volumetric reconstruction. First, a voxel (volumetric picture element) intensity threshold range of 600 to 2,610 units was applied to all slices to segment the

voxels corresponding to the area of interest. Manually, any excess voxels were removed and any voxels that pertained to the cortical bone not automatically selected were selected manually to obtain a closed shell of the femur cortical bone. The volumetric reconstruction of the cortical bone was exported from Amira in a WRL file format containing a point cloud of the cortical bone shape. The point cloud was converted into a surface model using RapidForm® (RapidForm, Seoul, South Korea) and exported in IGES file format.

Finite Element Modeling of the Three-Point Bending Experiments

All finite element analyses of the three-point bending tests were conducted using ABAQUS (Simulia, Providence, Rhode Island). Two types of FE models were used: parametric and actual bone models. The aim of the parametric analysis was to determine the correction factor of each bone, and, in these models, the geometry of the femur was simplified to that of a hollow elliptical-cylinder (see Appendix A for comparison of hollow elliptical and circular cylinders).

As seen in Figure 6, only a quarter of the cross-section of the femurs was included in the FE model to exploit symmetry and, therefore, reduce computational cost.

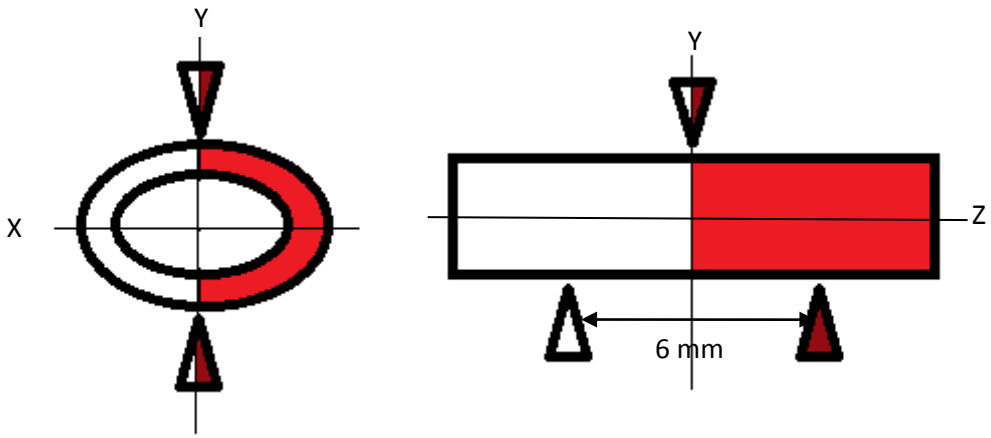

Figure 6. Schematic of the parametric model used in the finite element analysis of the three-point bending experiment.

The three-point bending support fixtures and upper fixture were modeled as analytically rigid solids. The femur model consisted of linear solid hexahedron elements with reduced integration formulation (see Appendix A for comparison of shell and solid elements). X- and z-axis symmetry boundary conditions were applied to the femur model. The reference point of the lower support was fixed. A y-axis displacement was applied to the reference point of the upper fixture and all other displacement and rotations at that point were fixed. The magnitude of this displacement was determined from the experiments as being the displacement at which the reaction force was 30% of the peak force. The interaction between each of the fixtures and the test femur was modeled as a surface-to-surface contact interaction, with a friction coefficient of 0.35 (Zand, Goldstein, & Matthews, 1983). The meshed model is shown in Figure 7. Mesh convergence tests were carried out to determine an appropriate element size (see Appendix B).

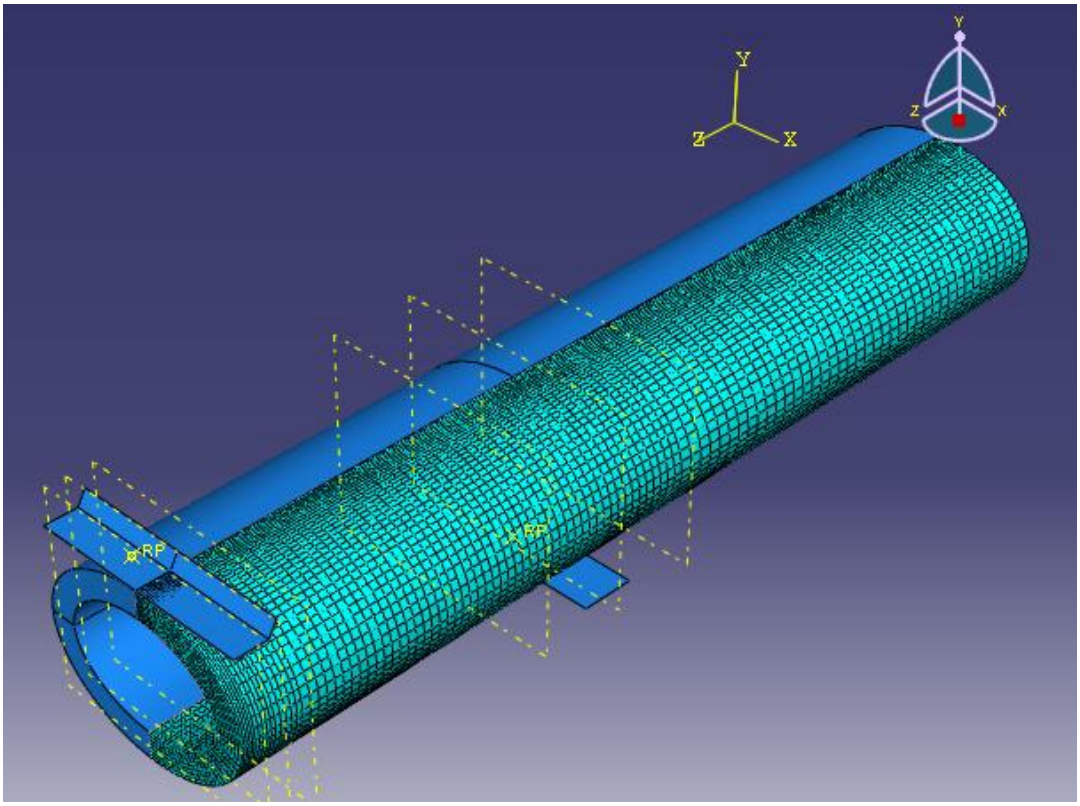

Figure 7. Finite element assembly model with mesh.

Correction Factor for the 2nd Degree Polynomial Material Model

For a three-point bending experiment, the theoretically derived or apparent elastic modulus is defined as

$$F = \frac{48E_{app}\delta I}{L^3} \tag{3.3}$$

where *F* is the applied force to the femur, *L* is the span, *δ* is the deflection of the femur, and *I* is the area moment of inertia of the femur. The subscript “app” indicates the fact that this elastic modulus is determined from experiments that violate the underlying assumptions of this theoretical equation.

The correction factor approach is based on the hypothesis that the error in the elastic modulus extracted from the three-point bending experiments using theoretical equation Eq. 3.2 depends on the real elastic modulus as well as on *I*. For elastic materials, this dependence is determined through a parametric FEA of three-point bending experiments with varying geometry and elastic modulus. Using the results of the parametric study, a comparison of true elastic modulus that is an input (E_{in}) and an apparent elastic modulus is obtained for each geometry.

The ratio of the E_{appFE} to the E_{in} is assumed to be a function of the true property and the area moment of inertia:

$$\frac{E_{appFE}}{E_{in}} = f(E_{in}, I) \tag{3.4}$$

Here, the function *f* is referred to as the error function. If *f* is determined computationally, then Eq. 3.3 may be used to determine the material parameters directly from the three-point bending experiments, which is practical and useful for many applications in which the concerns regarding assumptions of three-point bending are not negligible.

The form of *f* is determined through the following steps utilizing parametric FE analyses:

1. Determine a range for the parameters E_{in} and *I* (from literature and experiments) for the parametric analyses.
2. For the selected parameter range, carry out computational three-point bending experiments using the methods described in the previous section. For

each simulation with fixed values of E_{in} and I, compute the applied force-deflection data and then use Eq. 3.2 to determine E_{appFE}.

3. Parameterize $f = \frac{EappFE}{E_{in}}$ in terms of E_{in} and I. With f , the real elastic modulus E_{in} can be extracted directly from a three-point bending experiment using Eq. (3.2) by minimizing the quantity

$$\sum_{i=1}^{N}\left[F - \frac{48E_{in}\delta I}{L^3} f(E_{in}, I)\right]^2 \quad (3.5)$$

where N is the number of data-points in a given bending experiment and F is the experimental applied force.

Validation of Finite Element Model of the Three-Point Bending Experiment

In order to validate the FE model of the three-point bending experiment, a copper wire was used for FE and actual three-point bending experiments. Then, applied force-displacement data from FE and actual experiments were compared to determine if the modeling technique is valid.

Three-point bending experiments were performed on 2 mm diameter copper wire with a length of 20 mm, dimensions that are comparable to those of the murine femur. The wire was tested using an Instron 33R (Instron, Norwood, MA) at a rate of 2mm/sec to a 40% decline in maximum load. Load magnitude and displacement data were collected by the Bluehill Materials Testing Software (Instron, Norwood, MA). The test was performed on 12 samples. For the first six, the span was held at 6 mm; for samples 7-12 the span was held at 8 mm.

The same FE model used for the femur bend tests was used for the copper wire bend tests with minor changes. The cylinder was no longer hollow and it had a circular cross-section and the diameter was set to 2 mm. The same

boundary conditions were applied to the copper model as in the femur model. The reference point of the lower support was again fixed, but the displacement load applied to the reference point of the upper fixture was changed to -0.139 mm to reflect the experimental data. The interaction between the fixtures and the copper was still modeled as surface-to-surface contact interactions with a new friction coefficient of 0.53 (Friction and Coefficients of Friction, n.d.). The elastic modulus applied to the model was 126 GPa (within the range of accepted values for copper) (Young Modulus of Elasticity, n.d).

Statistical Analysis

All statistical analysis performed comparing the study groups were using student's t-tests for samples with unequal samples sizes and unequal variances. The *t* statistic to test whether the population means are different was calculated as follows:

$$t = \frac{\bar{\bar{X}}_1 - \bar{X}_2}{s_{\bar{X}_1 - \bar{X}_2}} \tag{3.6}$$

where $\bar{X}_1$ and $\bar{X}_2$ are the sample means from populations 1 and 2 and $s_{\bar{X}_1 - \bar{X}_2}$ is given by the expression

$$s_{\bar{X}_1 - \bar{X}_2} = \sqrt{\frac{s_1^2}{n_1} + \frac{s_2^2}{n_2}} \tag{3.7}$$

where s^2 is the unbiased estimator of the variance of the two samples and *n* is the sample size. In significance testing, the distribution of the test statistic was

approximated as being an ordinary student's t distribution with the degrees of freedom (DOF) calculated using the following

$$DOF = \frac{\left(s_1^2/n_1 + s_2^2/n_2\right)^2}{\left(s_1^2/n_1\right)^2/(n_1-1) + \left(s_2^2/n_2\right)^2/(n_2-1)} \quad (3.8)$$

CHAPTER 4: RESULTS

The aim of this work is to evaluate and compare the elastic modulus of genetically-modified murine femurs. To accomplish the aim, three major activities were undertaken: (1) mechanical testing of the murine femurs using three-point bending, (2) the development of a correction factor using a FE modeling to get a more accurate measure of the elastic modulus for each bone, and (3) the final characterization of the murine femurs and determination of whether there are differences between the four experimental groups.

Results of the Three-Point Bending Experiments on Murine Femurs

After completing the bend tests (Figure 8 and Table 2) and the geometric data were collected all possible material and geometric properties were compared between the four experimental groups: JHet, KHet, KJHet, and WT. These properties include peak force, 30% of the peak force, calculated elastic modulus using peak force, calculated elastic modulus using 30% of the peak force, area moment of inertia, cortical bone thickness, outer diameter of the major and minor axis, inner diameter of the major and minor axis, and the ratios of the outer to inner diameters. In the rest of the Results section, we will consider only the area moment of inertia and calculated elastic modulus using 30% of the peak force (Figures 9 and 10). 30% of the peak force was used based on the force-displacement curves that showed a linear relationship at this point for all samples.

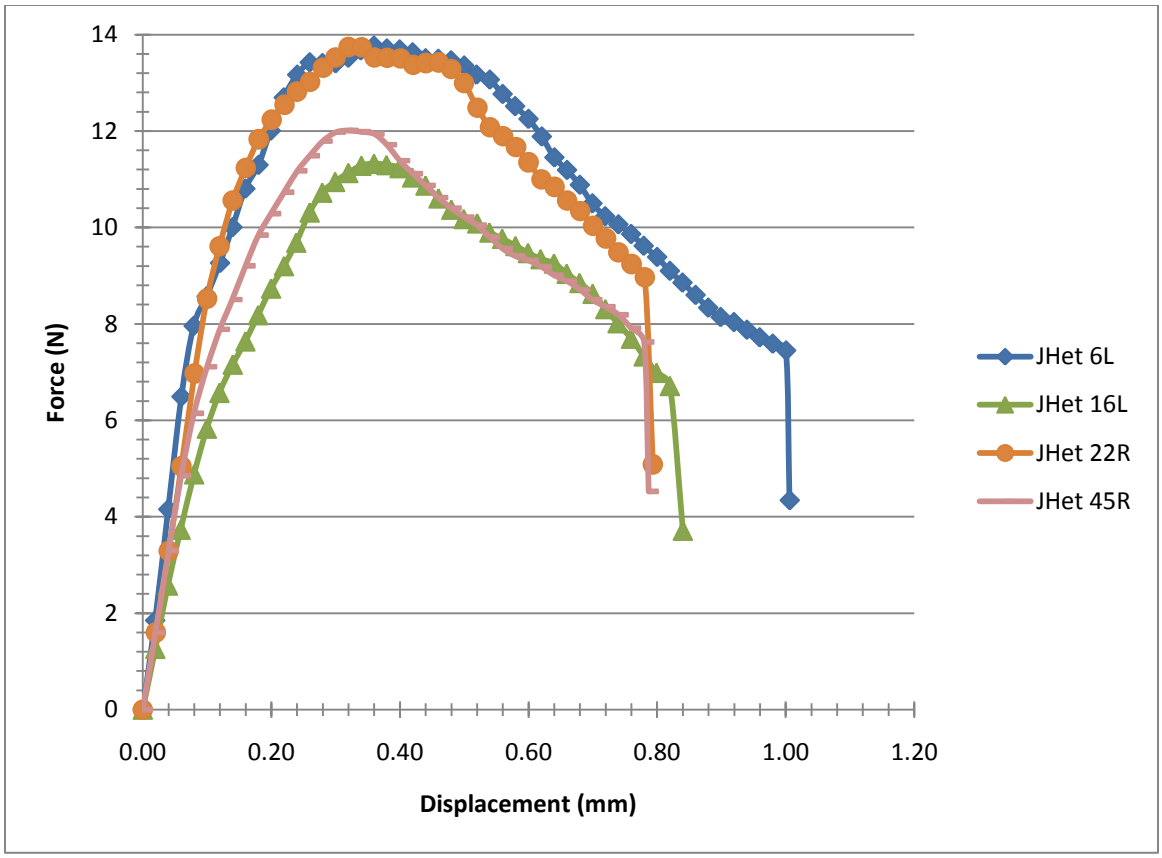

Figure 8. Experimental force-displacement curves from four JHet femurs

Table 2
Resulting Parameters Found from Three-Point Bending Experiments and Geometric Data for the Four JHet Femurs Plotted in Figure 8

Specimen	I (mm^4)	E_{app} (GPa)
JHet 6L	0.110	3.535
JHet 16L	0.097	2.710
JHet 22R	0.121	3.164
JHet 45R	0.121	2.487

It was found that there was only statistical difference when looking at two of the properties, namely elastic modulus using 30% of the peak force and the area moment of inertia. The apparent elastic modulus of KHet is significantly lower than that of each the other study groups. However, since this value is only the apparent elastic modulus and not the true elastic modulus this is not really the true comparison. The values need to be corrected for a true comparison of elastic modulii. Area moment of inertia for KHet is statistically larger than that for each of the other groups. It was also observed that the apparent elastic modulus values for the WT group were approximately 61-75% lower than literature results for comparable age murine femurs (Table 1).

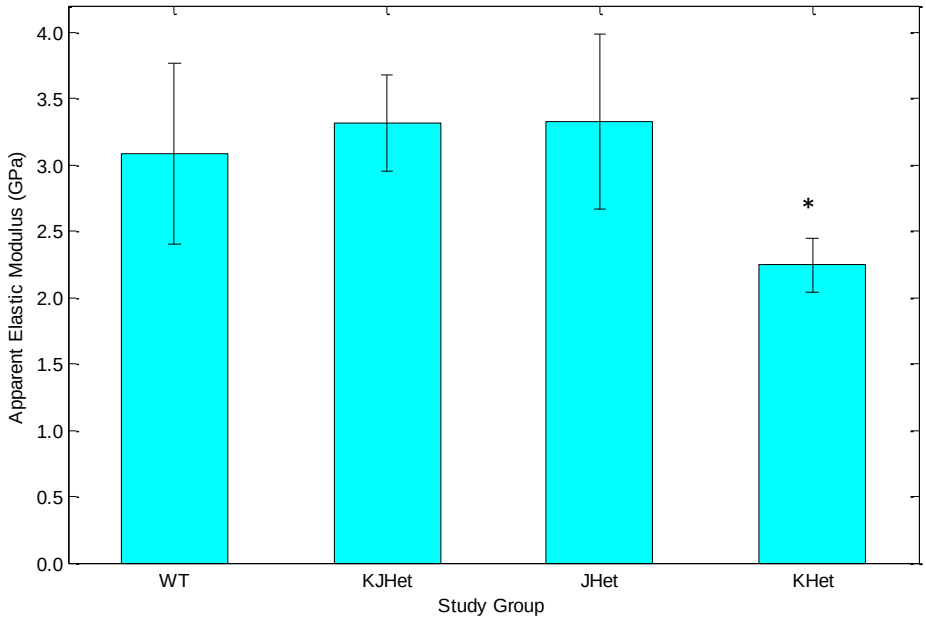

Figure 9. A summary of the apparent elastic modulus results (mean ± 1 standard deviation).* represents the experimental group that is statistically different from each of the other three, $p < 0.05$.

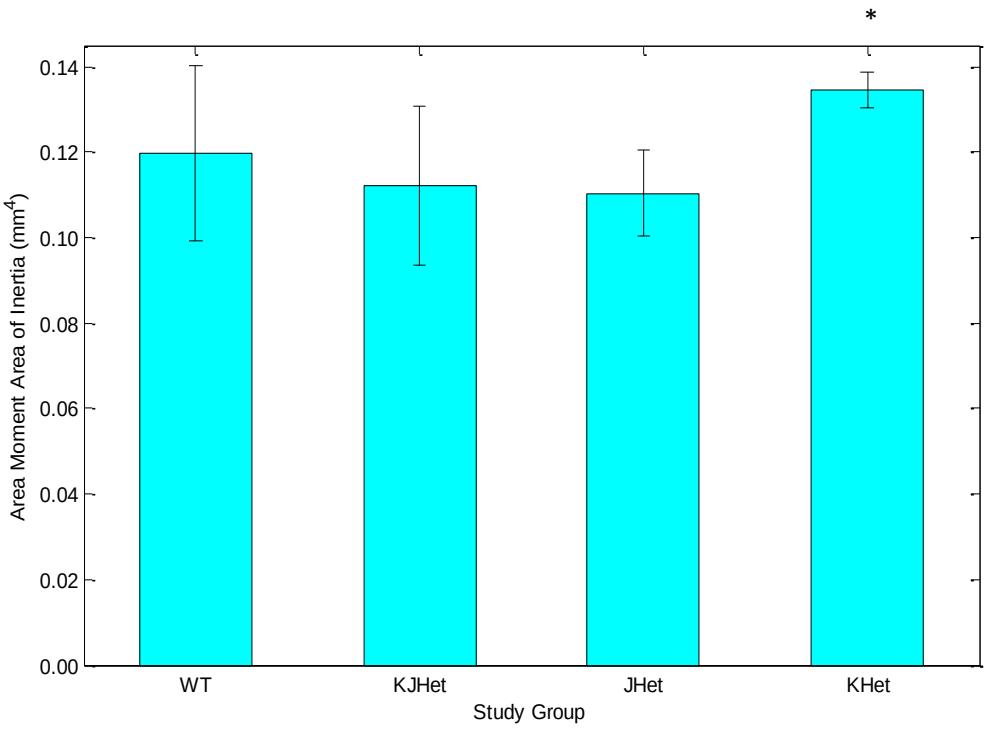

Figure 10. A summary of the area moment of inertia results (mean ± 1 standard deviation). * represents the experimental group that is statistically different from each of the other three groups, $p < 0.05$.

Validation of the FE Model

The results for one sample from the three-point bend testing and the equivalent FE model for the copper, using an input elastic modulus of 128 GPa, are shown in Figure 11.

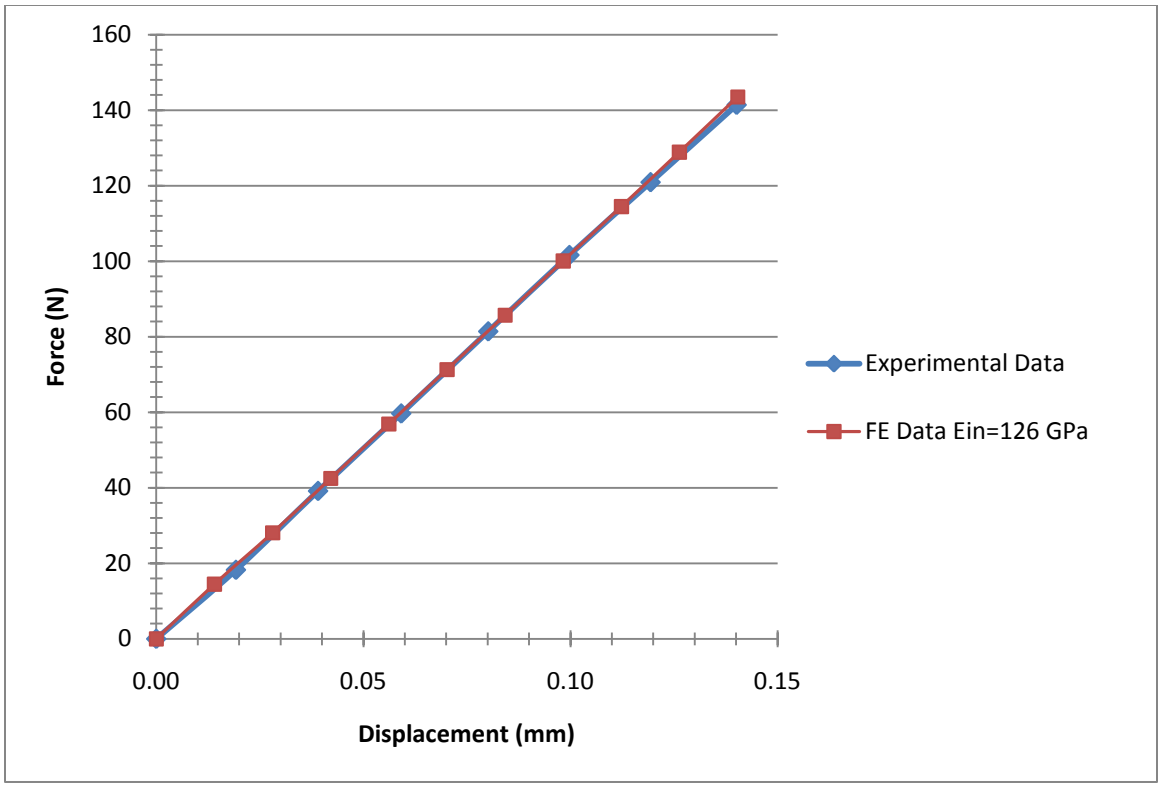

Figure 11. Comparison of the experimental and finite element data for the copper wire validation model (E_{in} = 126 GPa; span = 6 mm).

A chi-squared value was calculated to compare the experimental force-displacement data and the finite element force-displacement data. This value of 0.0998 signifies that there is a greater than 99.5% probability that the two curves are the same. The model is valid because it essentially produces the same force-displacement curve as the experimental one with the known elastic modulus of copper of 126 GPa.

Computational Determination of the Correction Factor

Once the FE model was validated for three-point bending experiment, FE analyses of the murine femur model were performed. The geometric model used assumed that the femur is symmetric about the x and z-axes, that the cortical

bone thickness is uniform, and that the geometry can be model as a cylinder. The preliminary analyses were conducted using parameters obtained during the mechanical testing. These analyses proved sensitive to a number of parameters that could be controlled in FE. Two parameters, namely (1) cortical bone thickness and (2) the input elastic modulus, were selected and their influence on the resulting force-displacement curves and in turn the apparent elastic modulii (E_{app}) of the murine femurs were determined.

The range of geometric parameters and elastic modulus was determined for the parametric FE analyses. Based on all of the apparent modulii obtained from three-point bending experiments (e.g., Table 2), a range for E_{in} was selected to be 4.75 GPa to 7.25 GPa. The geometrical parameter was determined based on observations regarding the bones tested. The outer major and minor axis diameters were held constant at 1.707 mm and 1.257 mm, respectively. These values are based on the means found in the experimental group's geometric data (e.g., Table 2). The outer diameters (OD) had a smaller variance when compared to the inner diameters; therefore, OD was selected to be held constant with the inner diameter changed with respect to the cortical bone thickness. The cortical bone thickness, t, ranges from 0.125 mm to 0.285 mm in increments of 0.016 mm. This results in an I range of 0.09 mm^4 to 0.15 mm^4 (e.g., Table 2).

Using the parametric FE results, the error function f is plotted against area moment of inertia in Figure 12 and against E_{in} in Figure 13. The error in the

apparent properties increases as the parameter *I* increases and is found to be independent of the parameter E_{in}.

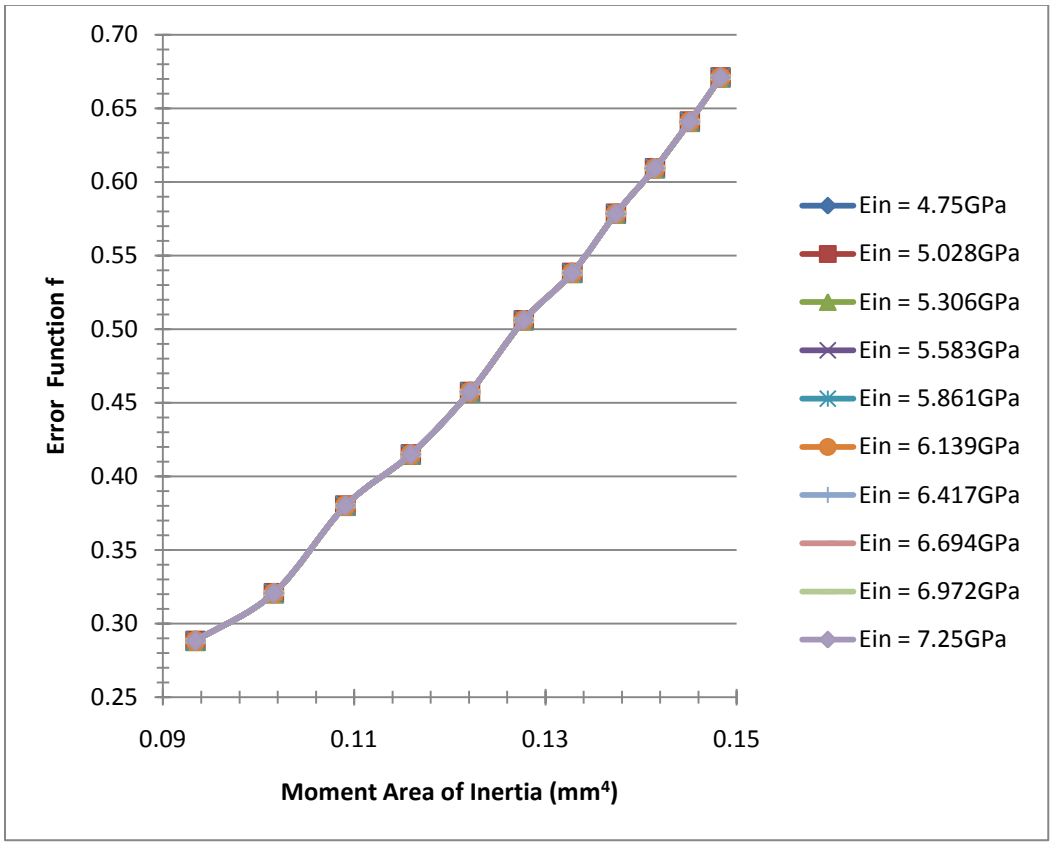

Figure 12. Plot of error function *f* as a function of *I* over the parameter range of E_{in}.

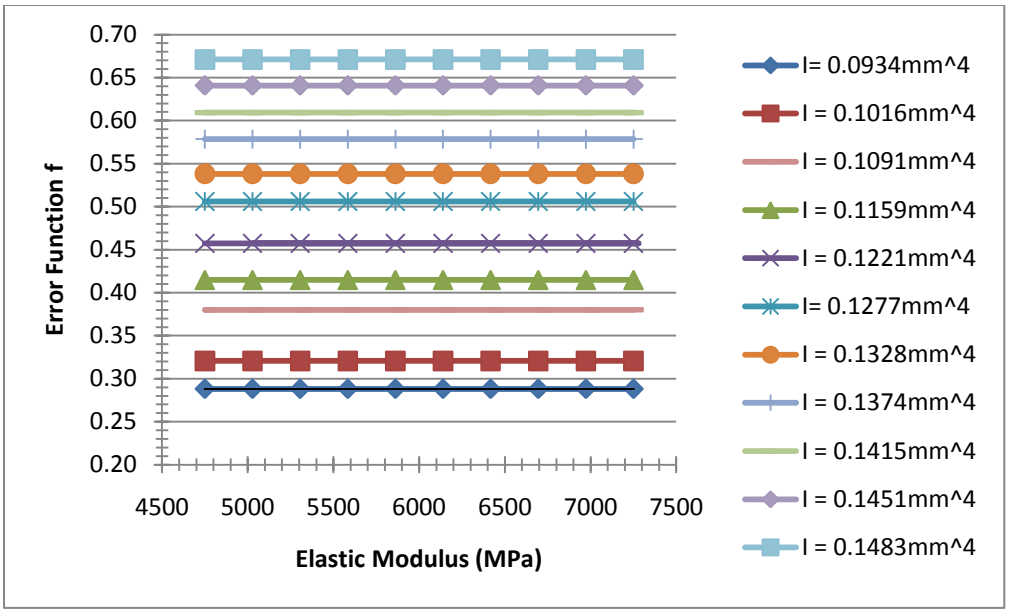

Figure 13. Plot of the error function *f* as a function of E_{in} over the parameter range of *I.*

Using the results of the parametric FE studies and analyzing the dependence of the error function on E_{in} and *I*, the following equation is found to describe the error function with a R^2 value of 0.999.

$$f(I) = 35.29I^2 - 1.5087I + 0.118 \quad (4.1)$$

Because this equation was obtained using FE and the theoretical equation Eq. 3.2, it can be utilized to compute the real underlying elastic modulus of tested specimens in three-point bending. But, first it is validated against experimental data as follows. Using the corrected material parameter *E* specified above, we carried out FE simulations of the three-point bending. The resulting force-displacement curves are compared with a force-displacement curve from the experiments (Figure 14).

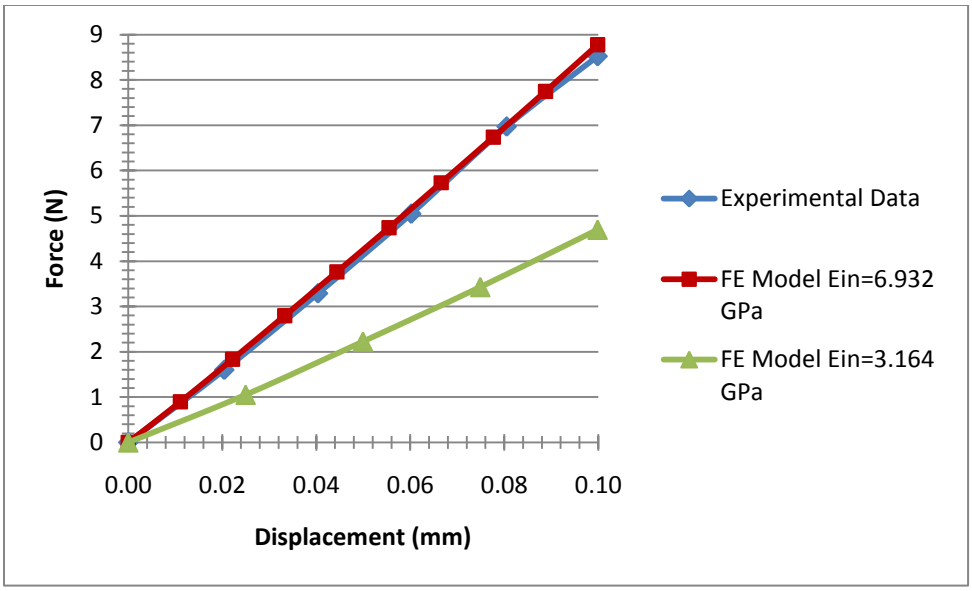

Figure 14. Comparison of the experimental and finite element force-displacement data for a murine femur sample.

A chi-squared value was calculated to compare the experimental force-displacement data and the finite element with corrected *E* force-displacement data. This value of 0.0278 signifies that there is a greater than 99.5% probability that the two curves are the same.

Statistical Analysis of Corrected Data

Equation 4.1 was used to compute the true elastic modulus (E_t) for each specimen (Figure 15 and Table 3). The results remained similar to the comparisons conducted on the E_{app} with results from the KHet group being statistically different from those of each of the other three experimental groups (Figure 15). There is a significant increase from *Eapp* to E_t in all groups. The values of the corrected elastic modulus for WT, JHet, and KJHet were within the range of relevant literature values (Table 1).

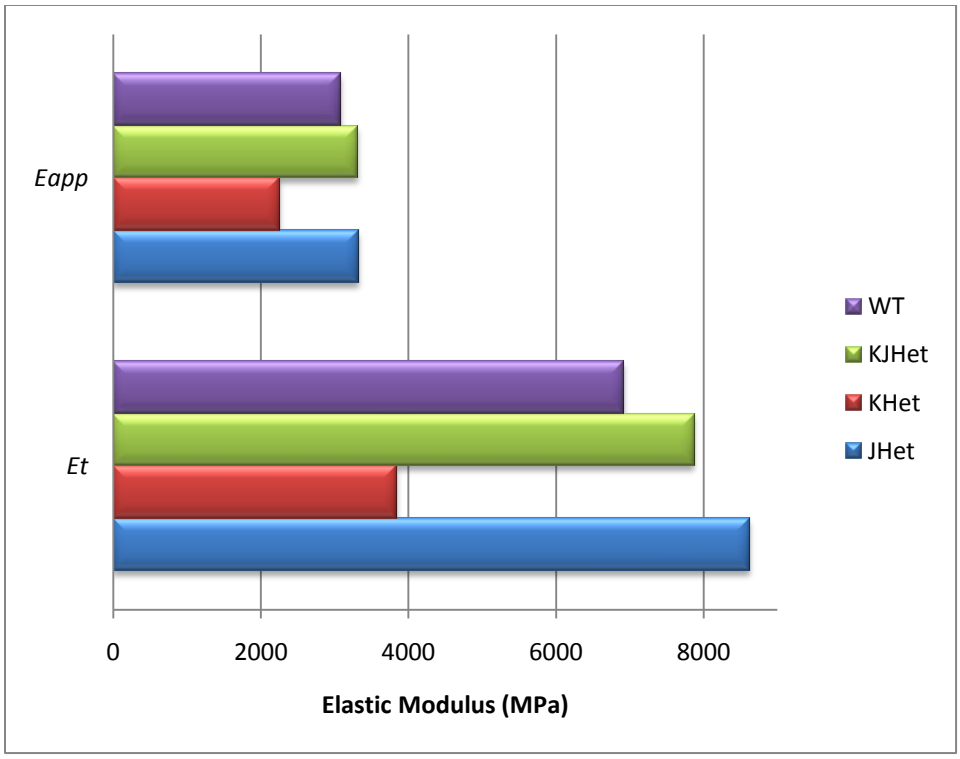

Figure 15. Summary of the mean *Eapp* and E_t values.

Table 3
Mean Error Function f Applied to Each of the Study Groups

Study Group	Mean *f*
JHet	0.386
KHet	0.585
KJHet	0.421
WT	0.446

CHAPTER 5: DISCUSSION

In this work, an evaluation of the global mechanical properties of genetically-modified murine femurs, specifically the elastic modulus, was performed. First, the mechanical three-point bend testing was performed. Because, the assumptions of the theoretical equation are violated, a numerical approach was utilized to take into account these challenges and determine the "real" elastic modulus form three-point bending experiments. The numerical approach involved a parametric FE model to determine an error function for the difference between real elastic modulus and the elastic modulus that the equation predicts. Using this equation, results from 48 three-point bending test were re-evaluated to obtain real elastic modulii. Finally, the corrected or adjusted, real E of the experimental tests were compared to determine whether statistically significant differences in the elastic modulus between the four experimental groups exist. The results in light of limitations and previous literature will be discussed in this chapter.

Aspect Ratio

In order to calculate the correct bone tissue properties from a bending test, the optimal aspect ratio of the bone (ratio of span length to outer diameter) should be > 20. If the aspect ratio is < 20, the bending test will generate a large shear deformation, thus reducing the elastic modulus. During the validation experiments, the span of the copper wire was modified and the importance of the

aspect ratio became more evident in bend testing; decreasing the aspect ratio from 4 to 3 lead to a 54.9% decrease in the calculated elastic modulus.

The aspect ratio of the murine femurs varied from 3.099 to 3.974, with a mean of 3.503. The aspect ratio of the KHet group is significantly smaller than that of each of the other three groups. This is because aspect ratio is inversely related to the cubed root of the area moment of inertia and the KHet group has a much larger area moment of inertia than each of the other three groups.

When the span length in the FE model was increased from 6.0 mm to 8.6 mm (changing the aspect ratio from 3.51 to 5.04), the error, calculated using the uncorrected beam theory equations, decreased from 53% to 22.6%. Due to the error dependency on span length, the correction factor, Eq. 4.1, is only applicable to experimental data using a span length of 6 mm. Appendix C has the complete results of an abbreviated parametric study conducted varying *I* and the span length *l*. Considering these results, there is a clear decrease in error as a function of *I* and *l*, but it is unclear what is the form of the error function. This can be explored in future work, but current work is conducted with all experiments having a 6 mm span, thus the error function is sufficient.

Indentation versus Deflection and Indentation at Supports

During the three-point bending tests, local deformation was observed at the supports and the upper fixture. This affects the resulting elastic modulus since at the recorded displacement, the bone does not really bend/deflect by that amount. In reality, the bone deflects in the presence of local deformation. Due to the inverse relationship between the elastic modulus and the deflection, this

results in a decrease in *Eapp* obtained using the theoretical equation Eq. 4.1, which does not account for local indentations.

Considering the results of the FE study, there is a difference in the deflection applied to the reference node and the resulting displacement values at the contacted nodes and the nodes further from the point of contact. If this were to be the full indentation of the bone, the applied displacement would be expected to be equal. However, there is more than a 5.7% difference in nodal displacement between the last node in contact with the upper fixture and its adjacent node. On the other hand, there is only a 0.14% variation in nodal displacement between all the nodes contacting the upper fixture. The same holds true at the lower support. Therefore, it is clear that the bone is not only bending, but there is also local deformation. It is suspected that this is true with the experimental work.

When the FE model was run with a span length of 8.6 mm (aspect ratio of 5.04), the local deformation due to the upper fixture decreased to 3.7% and decreased to 0.5% at the lower supports, which underscores the need for longer span length in whole bone testing. But, unfortunately, for small bones the span is limited to a small value.

Three out of the forty-eight femurs had excessive connective tissue. At the time of testing, there did not appear to be any noticeable difference in the force-displacement data for these femurs. It should be noted that this aspect was not modeled and, therefore, for those specific femurs, the error function may not be accurate.

Experimental Sample Size

The only group that was significantly different when looking the elastic modulus and area moment of inertia was also the group with the smallest sample size. Samples were received and tested on two different days with different average length of time frozen. The first set of femurs provided contained four femurs for each of the four study groups. The second set of samples contained eight femurs for the JHet group and eight for the KJHet group, sixteen femurs for the WT experimental group, and no KHet samples. There was not a statistically significant difference in the any of the parameters between the two sets, but there was a difference, which resulted in increased standard deviations in the JHet, KJHet, and WT groups. With the increased standard deviations, it made any differences between those three groups less significant.

Assumptions used in Developing the FE Model

There were four main assumptions used when developing the FE model of the murine femur:

1. it can be modeled as a hollow elliptical cylinder;
2. it has symmetry about the x and z axis;
3. it has uniform cross-sectional area; and,
4. the outer diameters are constant.

In Figure 14 are displayed the force-displacement curves of the experimental data and the data from the finite element model with the corrected *E*. Although the curves are statistically the same, there is a slight variance to them. This could be due to the assumptions made in developing the FE model; these assumptions

changed the area moment of inertia that the force was applied to. The slight variance could also be due to the difference in strain rates. The elastic modulus is linearly related to strain rate in the testing of bone. In the FE model, it was assumed that the problem was quasi-static; therefore, a strain rate was not specified and the displacement load was essentially applied instantaneously, which could lead to stiffer results.

Experimental Standardization

The study showed the dependency of the elastic modulus on different parameters during three-point bending. An error function that can be applied to experimental data resulting in a more accurate elastic modulus would allow for valid comparison of results from different studies. Using simple beam theory, three-point bending results can really only be used to compare within studies because there are too many parameters on which the elastic modulus is dependent. The three-point bending test is very simple and, with a reliable and valid error function, it becomes a viable option for the mechanical testing of whole bones.

Genetic Modification Effects

Based on the previous studies done at the cellular level (Xiao & Quarles, 2010), it was expected that the JHet group would have a significantly lower elastic modulus compared to the WT group. There had been no previous experiments specifically considering the differences in the KHet and KJHet groups; however, based on the function of the Kif3a gene it was hypothesized that those two groups lead to results similar to the JHet group (Xiao & Quarles,

2010). In the previous study, it was found that the KHet group had a significantly lower elastic modulus than the other three groups. This, in turn, leads to the conclusion that there is a greater effect on bone development from the loss-of-function in proteins required for cilia formation leading to polycystic kidney disease than from the deletion of the Pkd1 gene. Improved understanding of which specific gene mutations lead to abnormal bone development gives researchers a better understanding of how to treat bone degeneration disease, such as osteoporosis.

Significance of Study

FEA has been used to develop correction factors dependent on other parameters, such as aspect ratio (ratio of span length to outer diameter) (AR) and wall thickness ratio (ratio of inner diameter to outer diameter) (WTR). Using the mean AR and WTR for the WT mice used in the present study, the correction factor values were extrapolated from figures in previously published studies. The results of this comparison are displayed in Table 4 along with other experimental parameters that could affect the results of the study. The correction factor developed in the present study fell within the range of the previously published work; however, this study was unique in providing an equation that can be applied directly to experimental data.

Table 4
Comparison of Parameters Used in Correction Factor Studies

Age (weeks)	Bone	Gender	Murine Strain	Storage of Bone	FE Parameters	Correction Factor	Source
15	Femur	Female	C3H & B6	Frozen	*AR* & *WTR*	0.4-0.6	Van Lenth et al., 2008
-[a]	Femur	-[a]	-[a]	-[a]	*AR* & *WTR*	0.2-0.4	Kourtis & Beaupre, 2011
6	Femur	Male	-[a]	Frozen	*I*	0.45	Buechel, 2011

[a] Data not provided in the report.

CHAPTER 6: CONCLUSIONS

The overall aim of this thesis was to evaluate the mechanical differences between three different groups of genetically modified murine femurs and a control group. During the completion of this challenging task, efforts resulted in advances in the experimentation of the murine femurs in three-point bending. The following are the main conclusions of the study:

1. During three-point bending experiments of murine femurs, the correct aspect ratio for using standard beam theory equations cannot be achieved. This leads to increased local deformation and shearing deformation and, therefore, a significantly lower elastic modulus for the femur. The correction factor approach developed in this work is able to account for the local and shearing deformations at a span length of 6 mm.

2. The three-point bending experiments resulted in significantly lower apparent elastic modulus values than for comparable bones obtained using different test methods. The data from the experiments also showed a difference in elastic modulus and area moment of inertia for the KHet group compared to that for each of the other three study groups.

3. The correction factor was validated by inputting the corrected values of the elastic modulus into the FE model and comparing the resulting force-displacement data to those obtained from the experimental tests.

4. The corrected elastic modulii of the JHet, KJHet, and WT groups fall within the range of those of murine femurs of comparable age given in the literature.

5. The corrected elastic modulus of the KHet group was statistically lower than that of each of the other three study groups. This suggests that there is a greater effect on bone development from the loss-of-function in proteins required for cilia formation leading to polycystic kidney disease than from the deletion of the Pkd1 gene.

CHAPTER 7: RECOMMENDATIONS FOR FUTURE STUDY

The recommendations for future study are:

1. The correction factor obtained in the present work is not appropriate for span lengths other than 6 mm. Thus, there is scope for developing the correction factor into a more general equation that would allow the span length to be incorporated into the correction factor.

2. In the present work, area moment of inertia was one of the parameters studied, but it was only varied by changing the inner x and y diameters (by the same amount to maintain uniform thickness) and holding the outer diameters constant. For the femurs used in this work, this was acceptable because there was less variation in the outer diameters than in the inner diameters. This, however, is not likely to be the case for all whole bones. Thus, many different geometry parameters should be studied, examples being outer diameter, uniformity of thickness, and bone length.

References

Abaqus. (2007). Solid Isoparametric Quadrilaterals and Hexahedra. In *Abaqus Theory Manual.*

Bagi, C., Hanson, N., Andresen, C., Pero, R., Lariviere, R., Turner, C., et al.. (2006). The Use of Micro-CT to Evaluate Cortical Bone Geometry and Strength in Nude Rats: Correlation with Mechanical Testing, pQCT and DXA. *Bone, 38*, 136-144.

Bell, G. H., Cuthbertson, D. P., & Orr, J. (1941). Strength and Size of Bone in Relation to Calcium Intake. *Journal of Physiology*, *100*, 299-317.

Bending. (2011, February 17). Retrieved March 2011, from Wikipedia: http://en.wikipedia.org/wiki/Bending

Brkelmans, W. A., Poort, H. W., & Slooff, T. J. (1972). A New Method to Analyse the Mechanical Behaviour of Skeletal Parts. *Acta Orthopaedica Scandinavia, 43*, 301-317.

Burstein, A. H., & Frankel, V. H. (1971). Technical Note: A Standard Test for Laboratory Animal Bone. *Journal of Biomechanics, 4*, 155-158.

Chattah, N. L.-T., Sharir, A., Weiner, S., & Shahar, R. (2009). Determining the Elastic Modulus of Mouse Cortical Bone using Electronic Speckle Pattern Interferometry (ESPI) and Micro Computer Tomography: A New Approach for Characterizing Small-Bone Material Properties. *Bone*, *45*, 84-90.

Cook, M. J. (2008, February). *Flexor Surface of Right Femur*. Retrieved March 2011, from The Anatomy of the Laborator Mouse: http://www.informatics.jax.org/cookbook/figures/figure42.shtml

Cook, M. J. (2008, February). *Skeleton of LAC Grey Mouse*. Retrieved March 2011, from The Anatomy of the Laboratory Mouse: http://www.informatics.jax.org/cookbook/figures/figure10.shtml

Cowin, S. C. (2001). *Bone Mechanics Handbook*. Boca Raton: CRC Press.

Currey, J. D. (1999). What Determines the Bending Strength of Compact Bone? *The Journal of Experimental Biology, 202*, 2495-2503.

Draper, E., & Goodship, A. (2003). A Novel Technique for Four-Point Bending of Small Bone Samples with Semi-Automatic Analysis. *Journal of Biomechanics, 36*, 1497-1502.

Femur. (2011). Retrieved March 2011, from Encyclopedia Britannica: http://www.britannica.com/EBchecked/topic/204137/femur

Friction and Coefficients of Friction. (n.d.). Retrieved January 2011, from The Engeering Toolbox: http://www.engineeringtoolbox.com/friction-coefficients-d_778.html

Huebner, K. H., Dewhirst, D. L., & Smith, D. E. (2001). *The Finite Element Method for Engineers.* New York, NY: John Wiley & Sons.

Huiskes, R., & Chao, E. Y. (1983). A Survey of Finite Element Analysis in Orthopedic Biomechanics: The First Decade. *Journal of Biomechanics, 16*, 385-409.

Hutchinson, J. R. (2001). Shear Coefficients for Timoshenko Beam Theory. *Journal of Applied Mechanics, 86*, 87-92.

Ito, M., Nishida, A., Koga, A., Ikeda, S., Shiraishi, A., Uetani, M., et al.. (2002). Contribution of Trabecular and Cortical Components to the Mechanical Properties of Bone and Their Regulating Parameters. *Bone, 31*, 351-358.

Jamsa, T., Jalovaara, P., Peng, Z., Vaananen, H. K., & Tuukkanen, J. (1998). Comparison of Three-Point Bending Test and Peripheral Quantitative Computed Tomography Analysis in the Evaluation of the Strength of Mouse Femur and Tibia. *Bone, 23*, 155-161.

Kohles, S. S., Bowers, J. R., Vailas, A. C., & Vanderby, R. (1997). Ultrasonic Wave Velocity Measurement in Small Polymeric and Cortical Bone Specimens. *Journal of Biomedical Engineering, 119*, 232-236.

Kourtis, L. C., & Beaupre, G. S. (2011). Improving the Estimated of Elastic Modulus Derived from Three-Point Bending Test of Long Bones. *Orthopaedic Research Society 2011 Annual Meeting*, (Poster No. 2225). Long Beach, CA, Jan 13-16, 2011.

Mac Donald, B. J. (2007). *Practical Stress Analysis with Finite Elements.* Dublin: Glasnevin Publishing.

Martens, M., van Audekercke, R., de Meester, P., & Mulier, J. C. (1986). Mechanical Behaviour of Femoral Bones in Bending Loading. *Journal of Biomechanics, 19*, 443-454.

Miller, E., Delos, D., Baldini, T., Wright, T. M., & Camacho, N. P. (2007). Abnormal Mineral-Matrix Interactions are a Significant Contributor to Fragility in oim/oim Bone. *Calcified Tissue International, 81*, 206-214.

Nanoindentation. (n.d.). Retrieved March 2011, from Cornell University: http://www.nanoindentation.cornell.edu/Introduction/Nanoindentation-Introduction.htm

NCIB. (2009, August 7). *Osteogenesis imperfecta*. Retrieved March 2011, from PubMed Health: http://www.ncbi.nlm.nih.gov/pubmedhealth/PMH0002540/

NCIB. (2010, January 4). *Osteoporosis*. Retrieved March 2011, from PubMed Health: http://www.ncbi.nlm.nih.gov/pubmedhealth/PMH0001400/

NIH. (2011, January). *What is Osteoporosis*. Retrieved March 2011, from NIH Osteoporosis and Related Bone Diseases Nation Resource Center: http://www.niams.nih.gov/Health_Info/Bone/Osteoporosis/osteoporosis_ff.asp

Osteopenia Health Center. (2008, Novemeber 21). Retrieved March 2011, from WebMD: http://www.webmd.com/osteoporosis/tc/osteopenia-overview

Roan, E. (2007). Experimental and Multiscale Computational Approaces to the Nonlinear Characterization of Liver Tissue. *Ph.D. Dissertation*, University of Cincinnati.

Robling, A. G., & Turner, C. H. (2002). Mechanotransduction in Bone: Genetic Effects on Mechanosensitivity in Mice. *Bone, 31*, 565-569.

Saffar, K. P., JamilPour, N., & Rajaai, S. M. (2009). How Does the Bone Shaft Geometry Affect its Bending Properties? *American Journal of Applied Sciences, 6*, 463-470.

Schriefer, J., Robling, A., Warden, S., Fournier, A., Mason, J., & Turner, C. (2005). A Comparison of Mechanical Properties Derived from Multiple Skeletal Sites in Mice. *Journal of Biomechanics, 38*, 467-475.

Simkin, A., & Robin, G. (1973). The Mechanical Testing of Bone in Bending. *Journal of Biomechanics, 6,* 31-39.

Spatz, H.-C., O'Leary, E. J., & Vincent, J. F. (1996). Young's Moduli and Shear Moduli in Cortical Bone. *Proceeding of the Royal Society B: Biological Sciences, 263*, 287-294.

Tang, B., Hgan, A. H., & Lu, W. W. (2007). An Improved Method for the Measurement of Mechanical Properties of Bone by Nanoindentation. *Journal of Materials Science: Materials in Medicine, 18*, 1875-1881.

The University of Iowa. (2006, June 9). *Biomethodology of the Mouse*. Retrieved March 2011, from Animal Research: http://research.uiowa.edu/animal/?get=mouse

Three Point Flexural Test. (2011, February 8). Retrieved March 2011, from Wikipedia: http://en.wikipedia.org/wiki/Three_point_flexural_test

Turner, C. H. (1993). Mearsurment of the Young's Modulus in Bending Tests can be Highly Inaccurrate. *Jouranl of Orthopaedic Research, 11*, 462-463.

Turner, C. H., & Burr, D. B. (1993). Basic Biomechancial Measurments of Bone. *Bone, 14*, 595-608.

Turner, C. H., Hsieh, Y. F., Muller, R., Bouxsein, M. L., Rosen, C. J., McCrann, M. E., et al.. (2001). Variation in Bone Biomechanical Properties, Microstructure, and Density in BXH Recombinant Inbred Mice. *Journal of Bone and Mineral Research, 16*, 206-213.

Van Lenthe, H. G., Voide, R., Boyd, S., & Muller, R. (2008). Tissue Modulus Calculated from Beam Theory is Biased by Bone Size and Geometry: Implications for the use of Three-Point Bending Tests to Determine Bone Tissue Modulus. *Bone, 43,* 717-723

Wergedal, J. E., Sheng, M. H.-C., Ackert-Bicknell, C. L., Beamer, W. G., & Baylink, D. J. (2005). Genetic Variation in Femur Extrinsic Strength in 29 Different Inbred Strains of Mice is Dependent on Variations in Femur Cross-Sectional Geometry and Bone Density. *Bone, 36*, 111-122.

Xiao, Z., & Quarles, L. (2010). Role of the Polycytin-Primary Cilia Complex in Bone Development and Mechanosensing. *Annals of the New York Academy of Sciences, 1192*, 410-421.

Xiao, Z., Zhang, S., Cao, L., Qiu, N., David, V., & Quarles, L. (2010). Conditional Disruption of Pkd1 in Osteoblasts Results in Osteopenia Due to Direct Impariment of Bone Formation. *The Journal of Biological Chemistry, 285,* 1177-1187.

Xiao, Z., Zhang, S., Magenheimer, B., Luo, J., & Quarles, L. (2008). Polycysitn-1 Regulates Skeletogenesis through Stimulation of the Osteoblast-specific Transcription Factor RUNX2-II. *The Journal of Biological Chemistry, 283*, 12624-12634.

Xiao, Z., Zhang, S., Mahlios, J., Zhou, G., Magenheimer, B., Guo, D., et al.. (2006). Cilia-like Structures and Polycysitn-1 in Osteoblasts/Osteocytes and Associated Abnormalities in Skeletogenesis and Runx2 Expression. *The Journal of Biological Chemistry, 281,* 30884-30895.

Young Modulus of Elasticity for Metals and Alloys. (n.d.). Retrieved January 2011, from The Engineering Toolbox: http://www.engineeringtoolbox.com/young-modulus-d_773.html

Zand, M. S., Goldstein, S. A., & Matthews, L. S. (1983). Fatigue Failure of Cortical Bone Screws. *Journal of Biomechanics, 16*, 305-311.

APPENDIX A: Comparison of FE Modeling Techniques

The aim of this section is to determine if a murine femur can be modeled using shell elements instead of brick elements while under simulated three-point bend conditions. This model is also being compared to experimental data to determine if a hollow circular or hollow elliptical cylinder should be used to model a murine femur. The original femur geometry is shown in Figure 16.

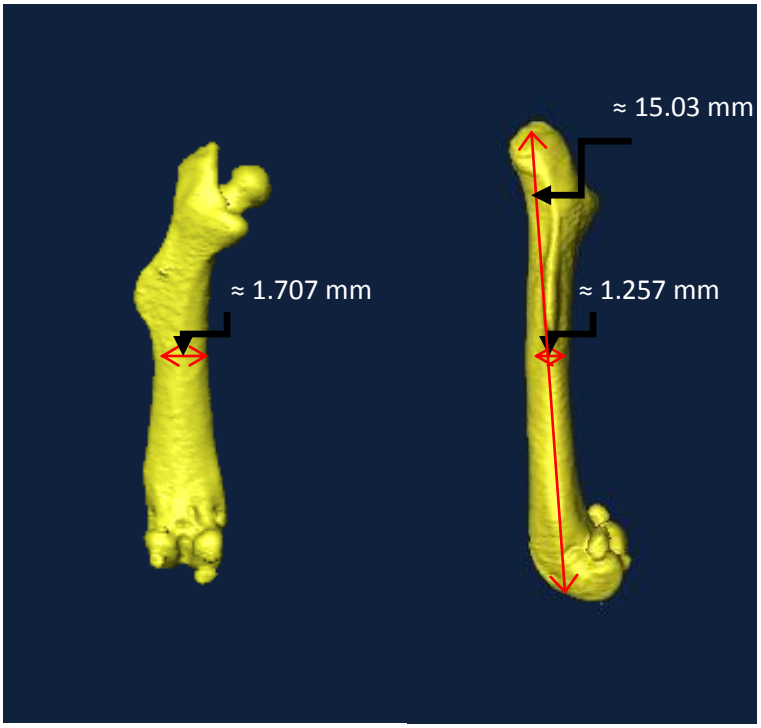

Figure 15. Original murine geometry.

Table 5 compares the geometry used in the models to that of the original murine femur. A distribution of elements used in the models is given in Table 6.

Table 5
Comparison of Original Murine Femur Geometry to Model Geometry

Model	Outer Diameter X-Direction	Outer Diameter Y-Direction	Inner Diameter X-Direction	Inner Diameter Y-Direction	Length
Murine Femur	1.707 mm	1.257 mm	1.24 mm	0.903 mm	14.7mm
Circular cross-section	1.482 mm	1.482 mm	1.072 mm	1.072 mm	7.35mm*
Elliptical cross-section	1.707 mm	1.257 mm	1.297 mm	0.847 mm	7.35mm*

*Length used in model after assuming z-symmetry

Table 6
Description of Elements Used in the Four Models

Model	Element Type	Number of Elements
Circular cross-section shell	S4R	3003
Elliptical cross-section shell	S4R	2821
Circular cross-section brick	C3D8R	16800
Elliptical cross-section brick	C3D8R	54600

Figures 17 and 18 show the contour plots of the Von Mises stress results for the shell element elliptical cross-section and brick element elliptical cross-section, respectively. The contour plots for the circular cross-section displayed similar stress distribution patterns, but with differences in magnitude.

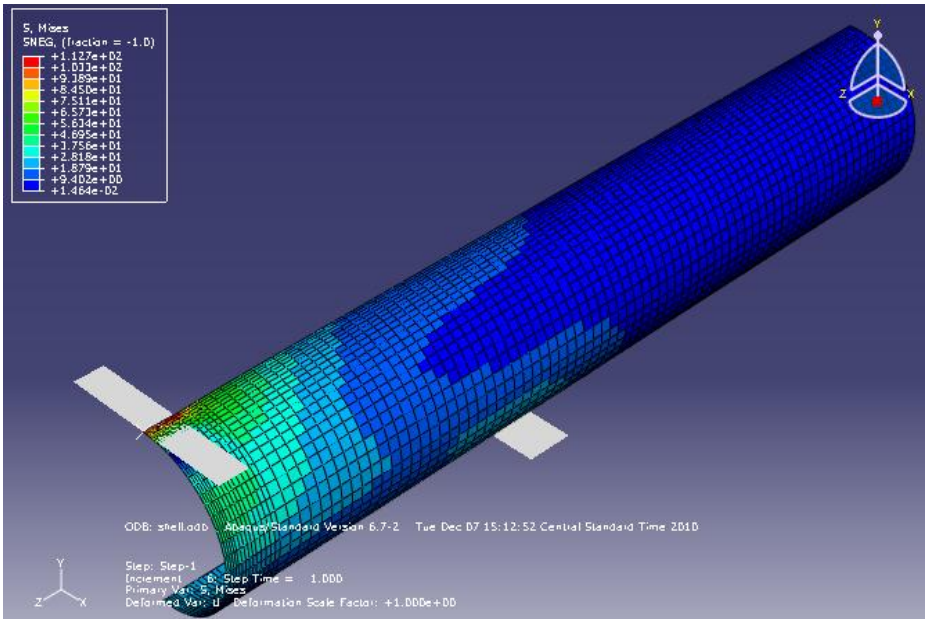

Figure 17. Von Mises stress results for the shell element elliptical cross-section model.

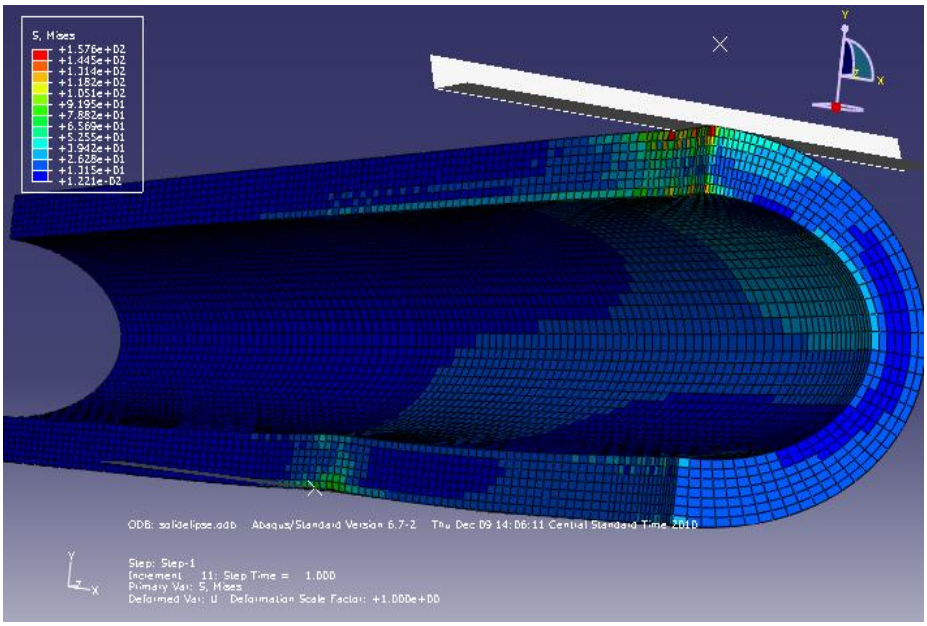

Figure 18. Von Mises stress results for the brick element elliptical cross-section model.

From the contour plots of the stress distribution, it is clear that the shell element model is not able to capture the difference in stress between the outer diameter and the inner diameter. Figure 18 clearly shows the variation in stress across the thickness of the model. We are unable to ignore this variation; therefore, the shell element model cannot be used in place of a brick element model. The contour plots for the circular cross-section model displayed a similar variation in stress across the thickness of the model. The theoretical results for the elliptical cross-section show that the elliptical model most closely models the experimental results. From this study, it can be concluded that, although, computationally expensive, the brick element elliptical cross-section model should be used in future work.

APPENDIX B: MESH CONVERGENCE STUDY

Mesh convergence tests were conducted on the FE models in this work to check the accuracy of the FE mesh. The convergence test was carried out by varying the element size at the point of contact on the model and monitoring the change in reaction force at the reference point of the upper fixture. Displayed in Figure 19 are the results of the convergence test run on the parametric model with an area moment of inertia of 0.128 mm^4. From the results of this test I used an element size of 0.02 was selected, resulting in the model having 54,600 elements.

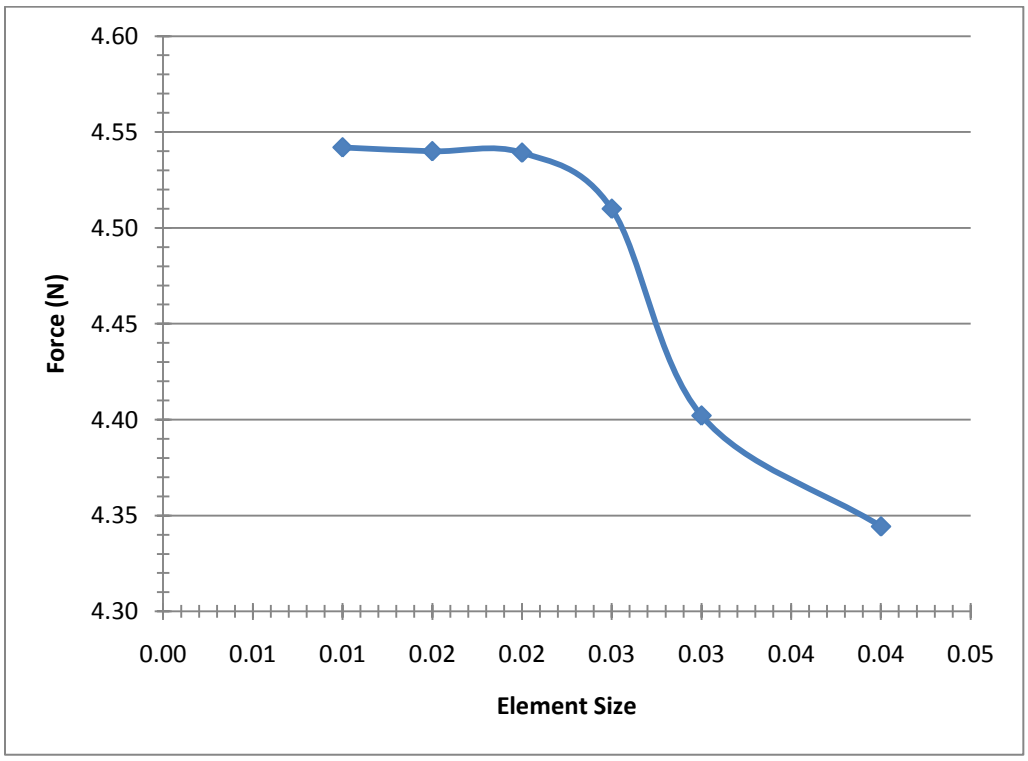

Figure 19. Results of the mesh convergence study perform on the parametric models.

APPENDIX C: Abbreviated Parametric Study Varying Area Moment of Inertia and Span Length

In order to calculate the correct bone tissue properties from a bending test, ideally, the bone's aspect ratio (ratio of span length to diameter) should be > 20. If the aspect ratio is < 20, the bending test will generate a larger shear deformation, thus reducing the elastic modulus. The easiest way to increase the aspect ratio is to increase the span length; however, with small bones, this is not always possible.

In this study, the correction factor approach is based on the hypothesis that the error in the elastic modulus extracted from the three-point bending experiments using theoretical equation Eq. 3.2 depends on the span length as well as on the area moment of inertia of the femur. This dependence for an elastic material is determined through a parametric finite element analysis of three-point bending experiments with varying geometry and span length (L). Using the results of the parametric study, a comparison of true elastic modulus that is an input (E_{in}) and an apparent elastic modulus is obtained for each geometry.

The ratio of the E_{appFE} to the E_{in} is supposed to be a function of the true property and the area moment of inertia:

$$\frac{E_{appFE}}{E_{in}} = g(L, I) \tag{C.1}$$

The form of *g* is determined the same as error function *f* as shown in the methods section. The results of the parametric study are shown in Figures 20 and 21.

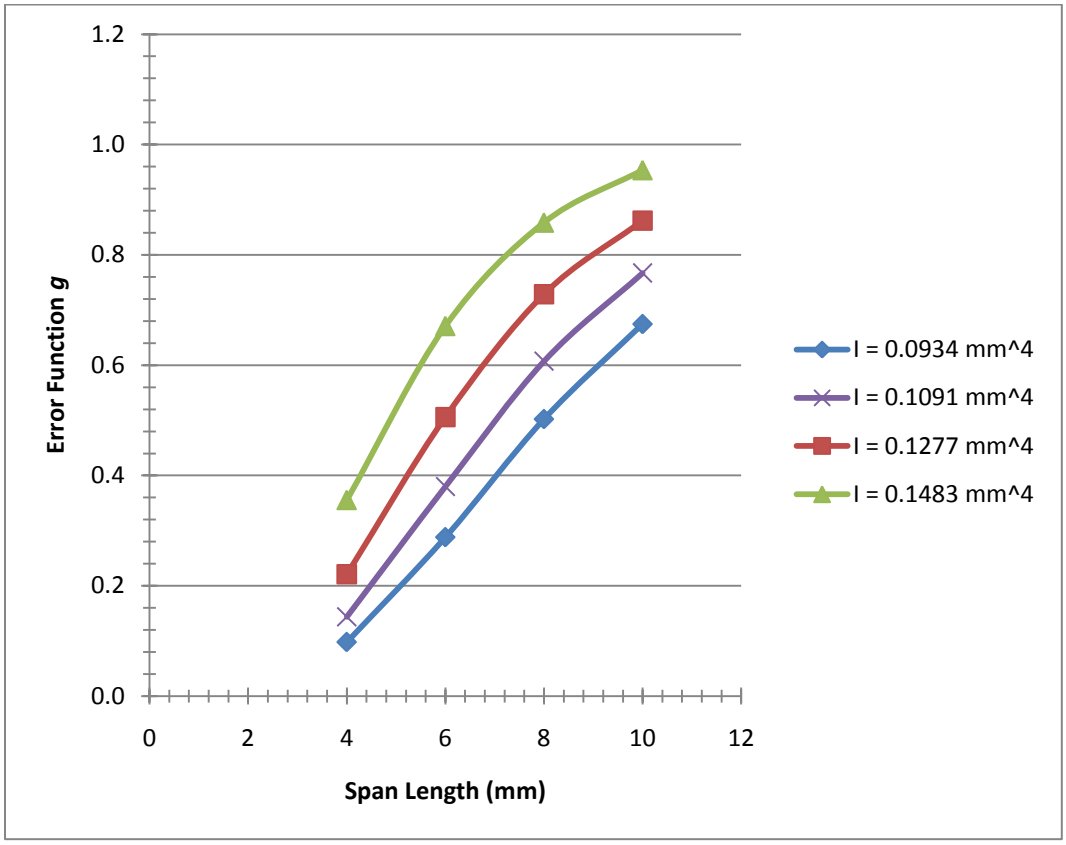

Figure 20. Plot of error function *g* as a function of *L* over the parameter range of *I*.

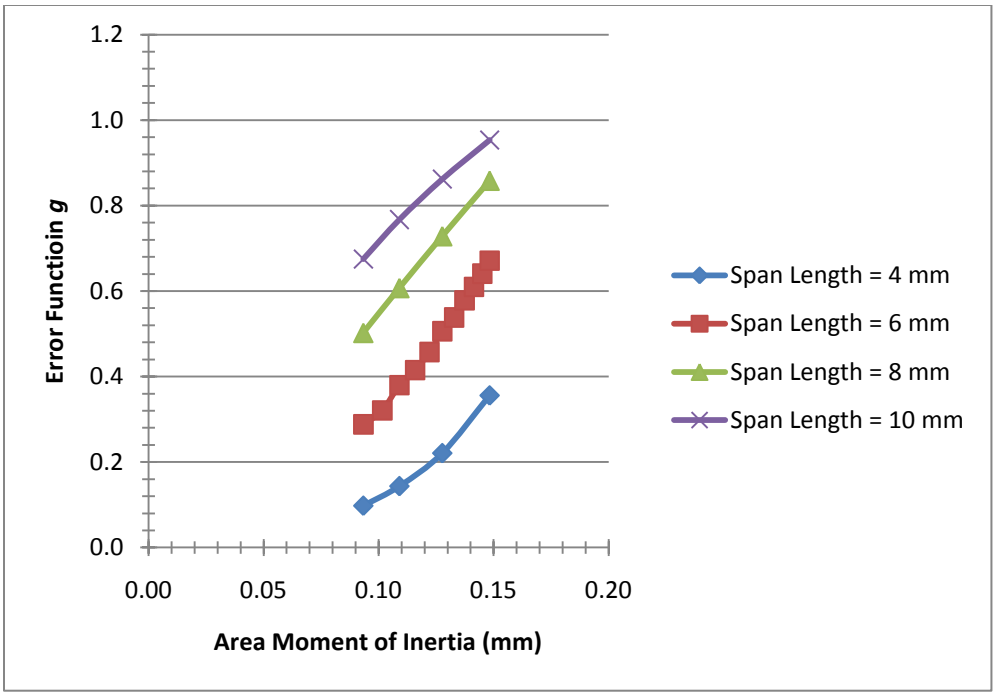

Figure 21. Plot of error function *g* as a function of *I* over the parameter range of *L*.

For all four area moment of inertia values tested, it appears that the error function as a function of span length may be a log function that will converge to the error function equaling one at larger span lengths. It is when the error function is a function of the area moment of inertia over varying span lengths that it is difficult to determine the correct form that the function should take. Considering Figure 21 at the two smaller span lengths (*L* = 4 mm and 6 mm), it appears that the function is a second-order polynomial. As the span length is increased, however, the concavity of the curve changes, making it difficult to determine how this function should be modeled. Wider ranges of both area moment of inertias and span lengths need to be studied in order to incorporate this dependence into the current error function, *f*.